Theoretical treatments of ultrafast electron transfer from adsorbed dye molecule to semiconductor nanocrystalline surface

Kuo Kan Liang, Chih-Kai Lin, Huan-Cheng Chang, Michitoshi Hayashi, and Sheng Hsien Lin

Citation: The Journal of Chemical Physics **125**, 154706 (2006); doi: 10.1063/1.2359445
View online: http://dx.doi.org/10.1063/1.2359445
View Table of Contents: http://scitation.aip.org/content/aip/journal/jcp/125/15?ver=pdfcov
Published by the AIP Publishing

Theoretical treatments of ultrafast electron transfer from adsorbed dye molecule to semiconductor nanocrystalline surface

Kuo Kan Liang[a)]
Division of Mechanics, Research Center for Applied Sciences, Academia Sinica, Taipei 115, Taiwan

Chih-Kai Lin and Huan-Cheng Chang
Institute of Atomic and Molecular Sciences, Academia Sinica, Taipei 106, Taiwan

Michitoshi Hayashi
Center for Condensed Matter Sciences, National Taiwan University, Taipei 106, Taiwan

Sheng Hsien Lin
Division of Mechanics, Research Center for Applied Sciences, Academia Sinica, Taipei 115, Taiwan;
Institute of Atomic and Molecular Sciences, Academia Sinica, Taipei 115, Taiwan;
and Department of Applied Chemistry, National Chiao-Tung University, Hsin-Chu 300, Taiwan

(Received 17 April 2006; accepted 8 September 2006; published online 18 October 2006)

In studying ultrafast electron transfer from a dye molecule to a nanosized semiconductor particle, pump-probe experiments are commonly used. In this system the electron transfer (ET) rate is faster than vibrational relaxation so that the ET rate should be described by a single-level rate constant and the probing signal (often in the form of time-resolved spectra) contains the contribution from the dynamics of both population and coherence (i.e., wave packet). In this paper, we shall present the theoretical treatments for femtosecond time-resolved pump-probe experiment and the dynamics of population and coherence by the density matrix method, and the calculation of single-level ET rate constant involved in a pump-probe experiment. As an application, we show the theoretical results using parameters extracted from experiments on a specific dye/semiconductor system.
 [DOI: 10.1063/1.2359445]

I. INTRODUCTION

Recently electron transfer (ET) between molecular adsorbents and semiconductor nanomaterials and surfaces has attracted considerable attention.[1–4] This interfacial ET from adsorbed molecules to the conduction band of semiconductor nanoparticles has been shown to take place within 100 fs. This indicates that in this system the ET is faster than the vibrational relaxation. Thus, the temperature is not defined in this ultrafast process and the thermal average ET rate constant cannot be used to describe this interfacial ET.

In addition to its fundamental importance, understanding the interfacial ET is also crucial to the development of numerous nanoparticle-based devices, such as molecular electronics[5,6] and solar cells based on composites of molecular and nanostructured semiconductor components.[1,7,8]

By using transient absorption spectroscopic techniques, time-resolved measurements of photoinduced interfacial ET with time constants shorter than 100 fs have become possible.[9–13] When ultrashort laser pulses are used in studying photoinduced ET (PIET), vibrational coherences (or vibrational wave packet) can often be observed and have indeed been observed in a number of dye-sensitized solar cell systems. This type of quantum beat has also been observed in ultrafast PIET in photosynthetic reaction centers.[14] It should be noted that when the PIET takes place in the time scale shorter than 100 fs, vibrational relaxation between the system and the heat bath is slower than the PIET; in this case we have the so-called vibrationally unrelaxed ET, which will be treated in this paper.

In studying ultrafast ET by femtosecond time-resolved experiments such as pump-probe experiments, the observed probe signals contain the information of the dynamics of not only the population but also the coherence of the system. Depending on the time scale and spectral ranges, the observed probe signals contain the dynamic information of either or both the reactant and product. A purpose of this paper is to present the theoretical method to calculate the femtosecond time-resolved probed spectra. To completely understand the mechanism of ultrafast ET for the dye-nanoparticle system, it is necessary to vary the pumping and probing wavelengths. In the 100 fs time scale, vibrational relaxation may still play some role in the ultrafast ET. It is the purpose of this paper to present (1) the theoretical description for ultrafast time-resolved absorption measurement which often exhibits quantum beat, (2) the theoretical treatment of nonrelaxed ET, and (3) the analysis of ultrafast time-resolved spectra experimentally observed.

To treat the PIET we shall employ the theoretical framework in which PIET is regarded as transitions between two potential surfaces and the potential surfaces are obtained by using the Born-Oppenheimer adiabatic approximation. Using this theoretical framework we shall show that for the case in which vibrational relaxation between the system and heat bath is much faster than the PIET so that vibrational equilibrium (i.e., thermal equilibrium) is established before PIET

[a)]Electronic mail: kkliang@sinica.edu.tw

takes place, the Marcus equation can be derived under certain approximations. For the case in which PIET is faster than vibrational relaxation, we have to deal with the calculation of the PIET rate originated from the vibronic levels prepared by the pumping laser, that is, the single-vibronic-level rate constant.

Thoss *et al.* have considered the similar kind of system and solve the Liouville equation of the vibronic process numerically via a so-called *self-consistent hybrid method* (SCH).[15] Their work represents an attempt to consider the vibrational degrees of freedom as well as the electronic degrees of freedom quantum mechanically at the same time. Some other workers have employed the so-called *nonadiabatic molecular dynamics* method to simulate the effect of nuclear motion on the ET process.[16,17] Willig *et al.* employed a similar Fano-Anderson model and solved the Schrödinger equation numerically.[18–21] They did not treat the semiconductor part explicitly like Thoss *et al.* did, and since it is the Schrödinger equation method that they have used, they could not consider the effect of pure dephasing. Their results are also limited to the one-vibrational-mode case. Sebastian and Tachiya[4] also studied such electron injection process by applying the Green's operator technique to the same model system. Rego and Batista[22] combined Car-Parrinello molecular dynamics (CPMD) method (which determines the time evolution of the structure of the dye-sensitized semiconductor nanoparticle) and the extended Hückel (EH) method (which determines the wave function of the system at each CPMD time step) to study the electron injection process in an all-atomic model. Both of these works compute the survival probability of the photoexcited state of the adsorbent. In the latter method, the wave function obtained from the EH computation is projected to the molecular orbitals of the adsorbent to calculate the survival probability, therefore the result does not reflect coherence dephasing dynamics. In both works, the transient spectra are not studied. In this article we shall provide an analytical expression for the single-vibronic-level electron transfer rate that can be used in the generalized linear response theory[14,23] which is based on the density matrix method and applied to pump-probe experiments. Multivibrational-mode case can be easily studied with this formulation.

This paper is organized as follows. In Sec. II we present the theoretical description of femtosecond pump-probe experiments based on the generalized linear response theory. Section III is concerned with the application of the density matrix method to the ultrafast ET dynamics. We show the derivation of vibrationally nonrelaxed ET rate constant in Sec. IV which will be followed by the application of theoretical results to the ultrafast ET in perylene-TiO_2 systems.

II. PUMP-PROBE EXPERIMENTS

A main feature of the interfacial ET under consideration takes place in the time scale shorter than 100 fs. Thus it is necessary to employ the laser with pulse duration $\sim$10 fs to study this ultrafast ET. From the uncertainty principle $\Delta E \cdot \Delta t \sim \hbar/2$ we can see that using this pulse duration, numerous vibronic states can be coherently pumped (or excited) and thus the probing signal in a pump-probe experiment will contain the information of the dynamics of both population and coherence (or phase). In other words, in order to obtain the information of ultrafast ET dynamics it is necessary to carefully analyze the probing signal (usually in the form of femtosecond time-resolved spectra). Theoretical description of ultrafast pump-probe experiment is presented in the following by using the generalized linear response theory (GLRT).

It has been shown that for the case in which the pumping and probing lasers do not overlap, one can use the generalized linear response theory.[14,23] In this section, we shall show how to apply the GLRT to calculate the ultrafast time-resolved spectra. For this purpose, we start from the stochastic Liouville equation to describe the equation of motion for the density matrix $\hat{\rho}(t)$ of the system embedded in a heat bath

$$\frac{d\hat{\rho}}{dt} = -i\hat{L}_0\hat{\rho} - \frac{i}{\hbar}[\hat{V}(t),\hat{\rho}] - \hat{\Gamma}\hat{\rho} = -i\hat{L}_0'\hat{\rho} - i\hat{L}'(t)\hat{\rho}, \tag{2.1}$$

$$\hat{L}_0' = \hat{L}_0 - i\hat{\Gamma},$$

where $\hat{L}_0$, $\hat{V}(t)$, and $\hat{\Gamma}$ represent the Liouville operator of the system, interaction between the system and probing laser, and the damping operator, respectively. We let

$$\hat{\rho} = e^{-it\hat{L}_0'}\hat{\sigma} \tag{2.2}$$

to obtain

$$\frac{d\hat{\sigma}}{dt} = -i\hat{\bar{L}}'(t)\hat{\sigma}, \tag{2.3}$$

where

$$\hat{\bar{L}}'(t) = e^{it\hat{L}_0'}\hat{L}'(t)e^{-it\hat{L}_0'}. \tag{2.4}$$

The equation of motion (EOM) of $\hat{\sigma}$ can be formally integrated,

$$\hat{\sigma}(t) = \hat{\sigma}_i - i\int_{t_i}^{t} d\tau \hat{\bar{L}}'(\tau)\hat{\sigma}(\tau), \tag{2.5}$$

where t_i is the initial time of the ET process and $\hat{\sigma}_i = \hat{\sigma}(t_i)$. In our case, the pump and probe pulses do not overlap each other. t_i is a moment after the pump pulse completely passed. Applying the perturbation method, the first order solution is given by

$$\hat{\rho}^{(1)}(t) = e^{-it\hat{L}_0'}\hat{\sigma}^{(1)}(t) = -i\int_{t_i}^{t} d\tau e^{-i(t-\tau)\hat{L}_0'}\hat{L}'(\tau)e^{-i(\tau-t_1)\hat{L}_0'}\hat{\rho}_i, \tag{2.6}$$

where $\hat{\rho}_i = \hat{\rho}(t_i)$.

Next we can calculate the polarization $\mathbf{P}(t)$. Consider the polarization due to the transitions between the two electronic manifolds $\{\ell\}$ and $\{m\}$, where $\{m\}$ is the upper manifold; to the first order, we have

$$\mathbf{P}(t) = \mathbf{P}^{(1)}(t) = \mathrm{Tr}[\hat{\boldsymbol{\mu}}\hat{\rho}^{(1)}(t)] = \sum_{\ell}\sum_{m}\rho_{\ell m}^{(1)}(t)\boldsymbol{\mu}_{m\ell}, \tag{2.7}$$

where

$$\rho_{\ell m}^{(1)}(t) = -\frac{i}{\hbar}\int_{t_i}^{t} d\tau e^{-i(t-\tau)\omega'_{\ell m}} \times \left\{ \sum_{m'} [V(\tau)_{\ell m'} e^{-i(\tau-t_i)\omega'_{m'm}} (\hat{\rho}_i)_{m'm}] - \sum_{\ell'} [V(\tau)_{\ell' m} e^{-i(\tau-t_i)\omega'_{\ell\ell'}} (\hat{\rho}_i)_{\ell\ell'}] \right\} \tag{2.8}$$

and $\boldsymbol{\mu}_{m\ell}$ is the transition dipole moment between m and ℓ states. Here, for example, $\omega'_{\ell k} \equiv \omega_{\ell k} - i\gamma_{\ell k}$ and $\gamma_{\ell k}$ is the dephasing constant. Since the system is initially prepared in the $\{\ell\}$ manifold, the first term in the bracket involving $(\hat{\rho}_i)_{m'm}$ can be removed. In other words,

$$\rho_{\ell m}^{(1)}(t) = \frac{i}{\hbar} e^{-it\omega'_{\ell m}} \sum_{\ell'} \left[e^{it_i\omega'_{\ell\ell'}} (\hat{\rho}_i)_{\ell\ell'} \int_{t_i}^{t} d\tau V(\tau)_{\ell' m} e^{i\tau\omega'_{\ell' m}} \right]. \tag{2.9}$$

The interaction V considered here is the dipole interaction of the system with the applied radiation field of the probing laser, that is,

$$V(\tau)_{\ell' m} = -\boldsymbol{\mu}_{\ell' m} \cdot [\mathbf{E}'_0(\omega) e^{-i\tau\omega} + \mathbf{E}_0(-\omega) e^{i\tau\omega}], \tag{2.10}$$

where ω is the frequency of the radiation field. In this case, we obtain

$$\rho_{\ell m}^{(1)}(t) = \frac{-1}{\hbar} \sum_{\ell'} \rho(\Delta t)_{\ell\ell'} \frac{\boldsymbol{\mu}_{\ell' m}}{\omega + \omega'_{\ell' m}} \cdot \mathbf{E}_0(-\omega) e^{it\omega}, \tag{2.11}$$

where $\Delta t = t - t_i$. The polarization is

$$\hat{P}(t) = \frac{-1}{\hbar} \sum_{\ell} \sum_{\ell'} \sum_{m} \rho(\Delta t)_{\ell\ell'} \frac{\boldsymbol{\mu}_{m\ell} \boldsymbol{\mu}_{\ell' m}}{\omega + \omega'_{\ell' m}} \cdot \mathbf{E}_0(-\omega) e^{it\omega} + \text{c.c.} \tag{2.12}$$

From Eq. (2.12) we can derive the susceptibility

$$\chi(\omega) = \frac{-1}{\hbar} \sum_{\ell} \sum_{\ell'} \sum_{m} \rho(\Delta t)_{\ell\ell'} \frac{\boldsymbol{\mu}_{\ell' m} \boldsymbol{\mu}_{m\ell}}{\omega + \omega'_{\ell m} + i\gamma_{\ell m}}. \tag{2.13}$$

As can be seen from Eq. (2.13), the dynamics of both population [i.e., $\rho_{\ell\ell}(\Delta t)$] and coherence [i.e., $\rho_{\ell\ell'}(\Delta t)$ with $\ell \neq \ell'$] is involved in the time-resolved measurement and Eq. (2.13) can be applied to optical absorption and stimulated emission. Furthermore, we recover the ordinary linear response theory when $\rho_{\ell\ell'} = 0$ and $\rho_{\ell\ell}$ represents the Boltzmann distribution.

Next we consider the effect of pumping laser. With a short-pulse pumping laser, both population excitation and coherence excitation can be created and the nonadiabatic processes such as photoinduced ET can take place afterwards. With a similar derivation as shown in this section we obtain the coherence created by the pumping laser with electric field $\mathbf{E}_{\text{pu}}$ and frequency ω_{pu} as

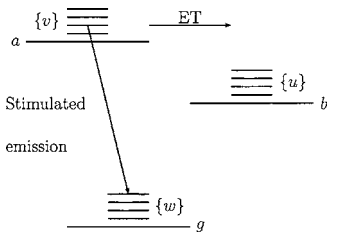

FIG. 1. Scheme of the pump-probe observation of ET process from a to b by monitoring the stimulated emission from a to the ground state g.

$$(\hat{\rho}_i)_{\ell\ell'} = \frac{\tau_{\text{pu}}^2}{\hbar^2} [\boldsymbol{\mu}_{\ell g} \cdot \mathbf{E}_{\text{pu}}^0(\omega_{\text{pu}})][\boldsymbol{\mu}_{g\ell'} \cdot \mathbf{E}_{\text{pu}}^0(-\omega_{\text{pu}})](\hat{\rho}_0)_{gg}, \tag{2.14}$$

where τ_{pu} denotes the pump-laser pulse duration. $\hat{\rho}_0$ is the density matrix of the system before the arrival of the pump pulse. Here it is assumed that initially only the g state is populated. $(\hat{\rho}_i)_{\ell\ell}$ is a particular case of $(\hat{\rho}_i)_{\ell\ell'}$ by setting $\ell' = \ell$.

Equation (2.14) shows that $(\hat{\rho}_i)_{\ell\ell'}$, which is involved in $\chi(\omega)$ in the GLRT, is proportional to $\mathbf{E}_{\text{pu}}^0(\omega_{\text{pu}})\mathbf{E}_{\text{pu}}^0(-\omega_{\text{pu}})$. This indicates that $\mathbf{P}(t)$ in the GLRT varies with $\mathbf{E}_p(\omega)$ and $\mathbf{E}_{\text{pu}}^0(\omega_{\text{pu}})\mathbf{E}_{\text{pu}}^0(-\omega_{\text{pu}})$. That is, according to the GLRT [see Eq. (2.13)] the linear susceptibility $\chi(\omega)$ due to the probing laser varies with time t through $\rho(\Delta t)_{\ell\ell'}$ (that is, the dynamics of the system) which in turn varies with $\mathbf{E}_{\text{pu}}(\omega_{\text{pu}})\mathbf{E}_{\text{pu}}(-\omega_{\text{pu}})$ of the pumping pulse, and this makes the $\chi(\omega)$ change into $\chi^{(3)}(\omega, -\omega_{\text{pu}}, \omega_{\text{pu}})$.

From the above discussion we can see that due to $\rho_{\ell\ell'}(\Delta t)$ the measurement of $\chi(\omega)$ will exhibit quantum beat; the beat frequency is $|\omega_{\ell\ell'}|$ while the beat width is approximately dependent on its dephasing constant. From Eq. (2.14) we can see that the ultrafast dynamics of population and coherence appears in $\rho(\Delta t)_{\ell\ell'}$ in which $(\hat{\rho}_i)_{\ell\ell'}$ play the role of initial condition, created by the pumping laser.

Next we shall apply the GLRT to analyze the femtosecond time-resolved spectra. Suppose that the probing process corresponds to stimulated emission (SE), the relations between the different electronic levels in this case are shown in Fig. 1. The ET is represented by $a \rightarrow b$ and SE is from a to g. Notice that in the Born-Oppenheimer adiabatic approximation

$$\psi_{a\mathbf{v}}(\mathbf{q}, \mathbf{Q}) = \Phi_a(\mathbf{q}, \mathbf{Q}) \Theta_{a\mathbf{v}}(\mathbf{Q}), \qquad \Theta_{a\mathbf{v}}(\mathbf{Q}) = \prod_j \chi_{av_j}(Q_j) \tag{2.15}$$

and

$$\psi_{g\mathbf{w}}(\mathbf{q}, \mathbf{Q}'') = \Phi_g(\mathbf{q}, \mathbf{Q}'') \Theta_{g\mathbf{w}}(\mathbf{Q}''), \qquad \Theta_{g\mathbf{w}}(\mathbf{Q}'') = \prod_j \chi_{gw_j}(Q''_j) \tag{2.16}$$

we find

$$\chi(\omega,t)=\frac{-1}{\hbar}\sum_{\mathbf{v}}\sum_{\mathbf{v}'}\sum_{\mathbf{w}}\rho(\Delta t)_{a\mathbf{v},a\mathbf{v}'}\frac{\boldsymbol{\mu}_{a\mathbf{v}',g\mathbf{w}}\boldsymbol{\mu}_{g\mathbf{w},a\mathbf{v}}}{-\omega+\omega_{a\mathbf{v},g\mathbf{w}}+i\gamma_{a\mathbf{v},g\mathbf{w}}}. \tag{2.17}$$

Here $\mathbf{q}$ denotes the electronic coordinates, and $\mathbf{Q}$ and $\mathbf{Q}''$ are the full sets of nuclear normal coordinates in the photoexcited (a) and ground (g) electronic states. Φ_a and Φ_g are the electronic wave functions. $\Theta_{a\mathbf{v}}$ and $\Theta_{g\mathbf{w}}$ are the full nuclear wave functions of the two different electronic states, each can be decomposed into products of single-mode wave functions $\Pi_j\chi_{av_j}$ and $\Pi_j\chi_{gw_j}$, respectively. Initially the coherence is created by the pumping process, i.e.,

$$(\hat{\rho}_i)_{a\mathbf{v},a\mathbf{v}'}=\frac{\tau_{\mathrm{pu}}^2}{\hbar^2}(\boldsymbol{\mu}_{a\mathbf{v},g\mathbf{0}}\cdot\mathbf{E}_{\mathrm{pu}}(\omega))(\boldsymbol{\mu}_{g\mathbf{0},a\mathbf{v}'}\cdot\mathbf{E}_{\mathrm{pu}}(-\omega))(\hat{\rho}_0)_{g\mathbf{0},g\mathbf{0}}. \tag{2.18}$$

From Eq. (2.17) we can see that the observed time-resolved spectra include the contributions from both population $\rho(\Delta t)_{a\mathbf{v},a\mathbf{v}}$ and vibrational coherence $\rho(\Delta t)_{a\mathbf{v},a\mathbf{v}'}$ where $\mathbf{v}\neq\mathbf{v}'$.

It should be noted that due to $\rho(\Delta t)_{a\mathbf{v},a\mathbf{v}'}$ the Fourier transform of $\chi(\omega,t)$ will yield a Lorentzian band shape with the bandwidth determined by the dephasing constant of $\rho(\Delta t)_{a\mathbf{v},a\mathbf{v}'}$ and the areas of different Fourier transform bands are approximately proportional to the Franck-Condon factors $|\langle\Theta_{a\mathbf{v}}|\Theta_{g\mathbf{0}}\rangle|^2|\langle\Theta_{a\mathbf{v}'}|\Theta_{g\mathbf{0}}\rangle|^2$. For the single displaced oscillator case, for example, $|\langle\chi_{a0}|\chi_{g0}\rangle|^2|\langle\chi_{a1}|\chi_{g0}\rangle|^2=Se^{-2S}$, where S is the Huang-Rhys factor, which will be further introduced in Sec. IV.

In the following we shall show how to calculate the band-shape function of femtosecond time-resolved spectra (that is, involving the contributions of both population and coherence dynamics) for the displaced harmonic potential surfaces. For allowed transitions $a\rightarrow n$ where n is the ground state g in the case of stimulated emission and it is a higher excited state in the case of induced absorption, Eq. (2.17) becomes

$$\chi(\omega,\Delta t)=-\frac{\boldsymbol{\mu}_{an}\boldsymbol{\mu}_{na}}{\hbar}\sum_{\mathbf{v}}\sum_{\mathbf{v}'}\sum_{\mathbf{u}}\rho_{a\mathbf{v},a\mathbf{v}'}\times(\Delta t)\frac{\langle\Theta_{a\mathbf{v}'}|\Theta_{n\mathbf{u}}\rangle\langle\Theta_{n\mathbf{u}}|\Theta_{a\mathbf{v}}\rangle}{\omega_{a\mathbf{v},n\mathbf{u}}-\omega+i\gamma_{a\mathbf{v},n\mathbf{u}}}, \tag{2.19}$$

which can be rewritten as

$$\chi(\omega,\Delta t)=i\frac{\boldsymbol{\mu}_{an}\boldsymbol{\mu}_{na}}{\hbar}\sum_{\mathbf{v}}\sum_{\mathbf{v}'}\rho_{a\mathbf{v},a\mathbf{v}'}(\Delta t)\times\int_0^\infty dt e^{-it(\omega-\omega_{an}-i\gamma_{an})}\prod_j G_{av_j',av_j}(t), \tag{2.20}$$

where

$$G_{av_j',av_j}(t)=\sum_{u_j}e^{it(v_j+1/2)\omega_j}e^{-it(u_j+1/2)\omega_j'}\langle\chi_{av_j'}|\chi_{nu_j}\rangle\times\langle\chi_{nu_j}|\chi_{av_j}\rangle. \tag{2.21}$$

In Appendix A, we show the detail of how to compute the time-correlation function (TCF) G_{av_j',av_j}. The result is

$$G_{av_j',av_j}=(-1)^{v_j+v_j'}\sqrt{\frac{v_j!v_j'!}{2^{v_j+v_j'}}}e^{iv_j\omega_jt}e^{-S_j(1-e^{-i\omega_jt})}\times\sum_{m_j=0}^{\min(v_j,v_j')}\frac{(2e^{-i\omega_jt})^{m_j}\kappa_j^{v_j+v_j'-2m_j}}{m_j!(v_j-m_j)!(v_j'-m_j)!}, \tag{2.22}$$

where

$$\kappa_j\equiv\sqrt{\beta_j}d_j(1-e^{-i\omega_jt}) \tag{2.23}$$

and $\beta_j=\omega_j/\hbar$.

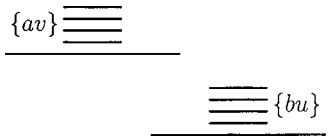

FIG. 2. Energy level scheme for $a\rightarrow b$.

III. ULTRAFAST DYNAMICS OF NONADIABATIC PROCESSES

In the previous section, we have shown how to apply the GLRT to calculate the ultrafast time-resolved absorption (or stimulated emission) spectra. In this section we shall apply the density matrix method to study the ultrafast dynamics of the system embedded in a heat bath. Due to the use of the ultrashort pulse in the pumping lasers the dynamical behaviors of both population and coherence have to be considered.

We shall consider the nonadiabatic transition $a\rightarrow b$ as shown schematically in Fig. 2, where a and b may denote the electronic states of D^*A and D^+A^-, respectively. To describe the dynamical processes of the system, we shall start with the stochastic Liouville equation

$$\frac{d\hat{\rho}}{dt}=-i\hat{L}_s\hat{\rho}-i\hat{L}'\hat{\rho}-\hat{\Gamma}\hat{\rho}, \tag{3.1}$$

where $\hat{L}_s$ derives from $\hat{H}_0$ of the system, and $\hat{L}'$ derives from the interaction $\hat{H}'$ that is responsible for the nonadiabatic processes using the Born-Oppenheimer adiabatic approximation. Here $\hat{\Gamma}$ denotes the damping operator due to the coupling between the system and heat bath. The generalized master equations (GMEs) of the nonadiabatic processes are given by

$$\frac{d\rho_{av,av}}{dt}=-\frac{i}{\hbar}\sum_u(H'_{av,bu}\rho_{bu,av}-\rho_{av,bu}H'_{bu,av})-(\hat{\Gamma}\hat{\rho})_{av,av}, \tag{3.2}$$

$$\frac{d\rho_{av,av'}}{dt}=-(i\omega_{av,av'}+\Gamma_{av,av'}^{av,av'})\rho_{av,av'}-\frac{i}{\hbar}\sum_u(H'_{av,bu}\rho_{bu,av'}-\rho_{av,bu}H'_{bu,av'}), \tag{3.3}$$

$$\frac{d\rho_{bu,av}}{dt} = -(i\omega_{bu,av} + \Gamma_{bu,av}^{bu,av})\rho_{bu,av} - \frac{i}{\hbar}\left(\sum_{v'} H'_{bu,av'}\rho_{av',av} - \sum_{u'} \rho_{bu,bu'}H'_{bu',av}\right), \tag{3.4}$$

where $\rho_{av,av}$, $\rho_{av,av'}$, and $\rho_{bu,av}$ represent the vibronic population, the vibrational coherence (or phase), and the vibronic coherence, respectively.

Equation (3.4) can be rewritten as

$$\frac{d\rho_{bu,av}}{dt} = -(i\omega_{bu,av} + \Gamma_{bu,av}^{bu,av})\rho_{bu,av} - \frac{i}{\hbar}H'_{bu,av}(\rho_{av,av} - \rho_{bu,bu}) - \frac{i}{\hbar}\left(\sum_{v'}^{v'\neq v} H'_{bu,av'}\rho_{av',av} - \sum_{u'}^{u'\neq u} \rho_{bu,bu'}H'_{bu',av}\right). \tag{3.5}$$

To the second-order approximation, by using the Laplace transformation method, $\rho_{bu,av}(t)$ can be eliminated from Eq. (3.2),

$$\frac{d\rho_{av,av}}{dt} = \frac{2}{\hbar}\sum_{u} \mathrm{Im}[H'_{av,bu}e^{-t(i\omega_{bu,av}+\gamma_{bu,av})}\rho_{bu,av}(0)] - (\hat{\Gamma}\hat{\rho})_{av,av} + \sum_{u}\int_0^t d\tau M(\tau)_{bu,av}[\rho_{bu,bu}(t-\tau) - \rho_{av,av}(t-\tau)], \tag{3.6}$$

where the memory kernel $M(\tau)_{bu,av}$ is given by

$$M(\tau)_{bu,av} = \mathrm{Im}\left[\frac{2i}{\hbar^2}|H'_{av,bu}|^2 e^{-\tau(i\omega_{bu,av}+\gamma_{bu,av})}\right]. \tag{3.7}$$

In the Markoff approximation Eq. (3.6) reduces to

$$\frac{d\rho_{av,av}}{dt} = \sum_{u} W_{bu,av}[\rho_{bu,bu}(t) - \rho_{av,av}(t)] - (\hat{\Gamma}\hat{\rho})_{av,av}, \tag{3.8}$$

where $W_{bu,av}$ denotes the rate constant for $av \leftrightarrow bu$,

$$W_{bu,av} = \int_0^\infty dt M(t)_{bu,av} = \frac{2}{\hbar^2}\frac{\gamma_{bu,av}}{\gamma_{bu,av}^2 + \omega_{bu,av}^2}|H'_{av,bu}|^2. \tag{3.9}$$

Here it is assumed that $\gamma_{bu,av}$ denotes the real part of $\Gamma_{bu,av}^{bu,av}$ and the imaginary part of $\Gamma_{bu,av}^{bu,av}$ is included in $\omega_{bu,av}$. Similarly we have

$$\frac{d\rho_{bu,bu}}{dt} = -\sum_{v} W_{bu,av}[\rho_{bu,bu}(t) - \rho_{av,av}(t)] - (\hat{\Gamma}\hat{\rho})_{bu,bu}. \tag{3.10}$$

Experimentally the dynamics of the product is also often measured.

Notice that in $(\hat{\Gamma}\hat{\rho})_{av,av}$ only vibrational relaxation is involved due to the coupling between the system and the heat bath, i.e.,

$$(\hat{\Gamma}\hat{\rho})_{av,av} = \sum_{v'} \Gamma_{av,av}^{av',av'}\rho_{av',av'} = \Gamma_{av,av}^{av,av}\rho_{av,av} + \sum_{v'}^{v'\neq v} \Gamma_{av,av}^{av',av'}\rho_{av',av'} = \sum_{v}{}' (\Gamma_{av,av}^{av',av'}\rho_{av',av'} - \Gamma_{av',av'}^{av,av}\rho_{av,av}). \tag{3.11}$$

It follows that

$$\frac{d\rho_{av,av}}{dt} = \sum_{u} W_{bu,av}[\rho_{bu,bu}(t) - \rho_{av,av}(t)] - \sum_{v}{}' (\Gamma_{av,av}^{av',av'}\rho_{av',av'} - \Gamma_{av',av'}^{av,av}\rho_{av,av}). \tag{3.12}$$

Similarly we have

$$\frac{d\rho_{bu,bu}}{dt} = -\sum_{v} W_{bu,av}[\rho_{bu,bu}(t) - \rho_{av,av}(t)] - \sum_{u}{}' (\Gamma_{bu,bu}^{bu',bu'}\rho_{bu',bu'} - \Gamma_{bu',bu'}^{bu,bu}\rho_{bu,bu}). \tag{3.13}$$

On the right-hand side of Eq. (3.12), the first summation and the first and second terms in the second summation describe the dynamical behaviors of $\rho_{av,av}$ due to the vibronic coherence dynamics, nonadiabatic transitions, and vibrational relaxation, respectively. Several cases can be considered. First, if the vibrational relaxation is much faster than electronic processes, then

$$\Gamma_{av,av}^{av',av'}\rho_{av',av'} = \Gamma_{av',av'}^{av,av}\rho_{av,av}, \tag{3.14}$$

i.e., principle of detailed balance, and if the heat bath maintains thermal equilibrium, then $\rho_{av,av}$ is related to the Boltzmann distribution P_{av} by

$$\rho_{av,av}(t) = \rho_a(t)P_{av}, \tag{3.15}$$

where $\rho_a(t)$ represents the total population of the system in the a electronic state. Similarly we have

$$\rho_{bu,bu}(t) = \rho_b(t)P_{bu}. \tag{3.16}$$

Using Eqs. (3.15) and (3.16), we can rewrite Eq. (3.12) as

$$\frac{d\rho_a}{dt} = (W_{b\to a}\rho_b - W_{a\to b}\rho_a), \tag{3.17}$$

where

$$W_{b\to a} = \sum_{v}\sum_{u} P_{bu}W_{bu,av} \tag{3.18}$$

and

$$W_{a\to b} = \sum_{v}\sum_{u} P_{av}W_{av,bu}, \tag{3.19}$$

i.e., thermal average rate constants. Here $W_{av,bu} = W_{bu,av}$.

Similarly we have

$$\frac{d\rho_b}{dt} = -(W_{b\to a}\rho_b - W_{a\to b}\rho_a). \tag{3.20}$$

Next if vibrational relaxation is much slower than electronic transition then

$$\frac{d\rho_{av,av}}{dt} = -W_{av}\rho_{av,av} + \sum_u W_{bu,av}\rho_{bu,bu}, \tag{3.21}$$

where W_{av} denotes the single-vibronic-level rate constant

$$W_{av} = \sum_u W_{av,bu}. \tag{3.22}$$

Similarly we have

$$\frac{d\rho_{bu,bu}}{dt} = -W_{bu}\rho_{bu,bu} + \sum_u W_{av,bu}\rho_{av,av}, \tag{3.23}$$

where

$$W_{bu} = \sum_v W_{bu,av}. \tag{3.24}$$

The results presented in this section are very general and can be applied to internal conversion (IC), intersystem crossing (ISC), photoinduced energy transfer (EET), and photoinduced electron transfer (ET).

The coherence dynamics of products is often observed and will be treated in the following. Consider the electronic levels a and b shown in Fig. 2. We have

$$\frac{d\rho_{bu,bu'}}{dt} = -(i\omega_{bu,bu'} + \gamma_{bu,bu'})\rho_{bu,bu'} - \frac{i}{\hbar}\sum_v (H'_{bu,av}\rho_{av,bu'} - \rho_{bu,av}H'_{av,bu'}), \tag{3.25}$$

where

$$\frac{d\rho_{av,bu'}}{dt} \cong -(i\omega_{av,bu'} + \gamma_{av,bu'})\rho_{av,bu'} + \frac{i}{\hbar}H'_{av,bu'}\rho_{av,av} \tag{3.26}$$

and

$$\frac{d\rho_{bu,av}}{dt} \cong -(i\omega_{bu,av} + \gamma_{bu,av})\rho_{bu,av} - \frac{i}{\hbar}H'_{bu,av}\rho_{av,av}. \tag{3.27}$$

It follows that we have, approximately,

$$\frac{d\rho_{bu,bu'}}{dt} = -(i\omega_{bu,bu'} + \gamma_{bu,bu'})\rho_{bu,bu'} + \frac{1}{\hbar^2}\sum_v \rho_{av,av}H'_{bu,av}H'_{av,bu'} \times\left(\frac{1}{i\omega_{av,bu'} + \gamma_{av,bu'}} + \frac{1}{i\omega_{bu,av} + \gamma_{bu,av}}\right). \tag{3.28}$$

Equation (3.28) can be solved by first solving for $\rho_{av,av}(t)$ and then substituting the resulting $\rho_{av,av}(t)$ into Eq. (3.28) to obtain the product coherence $\rho_{bu,bu'}(t)$. Another way to create the product vibrational coherence is due to the anharmonic coupling U in the product states

$$\frac{d\rho_{bu,bu'}}{dt} = -(i\omega_{bu,bu'} + \gamma_{bu,bu'})\rho_{bu,bu'} - \frac{i}{\hbar}U_{bu,bu'}(\rho_{bu',bu'} - \rho_{bu,bu}). \tag{3.29}$$

In Eq. (3.25), the product vibrational coherence is created out of the vibronic coherence between a and b. In contrast, in Eq. (3.29), the populations of the product vibrational levels are created first, and then anharmonic effect creates coherence between them.

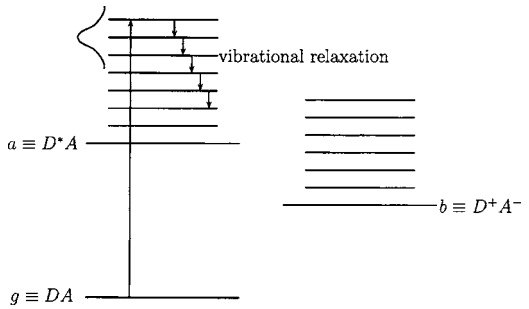

FIG. 3. Effect of vibrational relaxation on photoinduced ET.

IV. SINGLE-VIBRONIC-LEVEL ELECTRON TRANSFER RATE CONSTANT

Figure 3 demonstrates the effect of vibrational relaxation on photoinduced ET in an ultrashort pulse experiment where more than one vibronic levels are coherently pumped and only the single-level rate constant plays an important role in ultrafast ET.

There are three types of rate constants appearing in Sec. III, that is, $W_{bu,av}$, the state-to-state rate constant, $W_{a\mathbf{v}}$ (or $W_{b\mathbf{u}}$), the single-vibronic-level rate constant and $W_{a\to b}$ (or $W_{b\to a}$), the thermal average rate constant. However, as shown in Sec. II, only $W_{a\mathbf{v}}$ (or $W_{b\mathbf{u}}$) are involved in femtosecond time-resolved measurements (see Fig. 2). The calculation of $W_{a\mathbf{v}}$ (or $W_{b\mathbf{u}}$) will be given in this section. In the Born-Oppenheimer adiabatic approximation, the molecular-system wave functions $\psi_{a\mathbf{v}}$ and $\psi_{b\mathbf{u}}$ can be written in terms of the electronic wave functions $\Phi_a(\mathbf{q},\mathbf{Q})$ and $\Phi_b(\mathbf{q},\mathbf{Q})$ and vibrational (rovibrational) wave functions $\Theta_{a\mathbf{v}}(\mathbf{Q})$ and $\Theta_{b\mathbf{u}}(\mathbf{Q})$. In this case, $H'_{a\mathbf{v},b\mathbf{u}}$ can be written as

$$H'_{a\mathbf{v},b\mathbf{u}} = \langle\Theta_{a\mathbf{v}}(\mathbf{Q})|H'_{ab}|\Theta_{b\mathbf{u}}(\mathbf{Q})\rangle, \tag{4.1}$$

where H'_{ab} represents the electronic matrix elements, $H'_{ab}(\mathbf{Q})$. In most nonadiabatic processes (except IC), $H'_{ab}(\mathbf{Q})$ can be expanded in terms of vibrational coordinates $\{Q_j\}$. For the case in which $H'_{ab}(\mathbf{0})$ is nonzero, the first-order term can be neglected, i.e., $H'_{ab}(\mathbf{Q}) = H'_{ab}(\mathbf{0})$. This is usually called the Condon approximation. In this case, we have

$$W_{b\mathbf{u},a\mathbf{v}} = \frac{2\pi}{\hbar^2}|H'_{ab}(\mathbf{0})|^2|\langle\Theta_{a\mathbf{v}}|\Theta_{b\mathbf{u}}\rangle|^2 D(\omega_{b\mathbf{u},a\mathbf{v}}), \tag{4.2}$$

$$W_{a\mathbf{v}} = \frac{2\pi}{\hbar^2}|H'_{ab}(\mathbf{0})|^2 \sum_{\mathbf{u}} |\langle \Theta_{a\mathbf{v}}|\Theta_{b\mathbf{u}}\rangle|^2 D(\omega_{b\mathbf{u},a\mathbf{v}}), \tag{4.3}$$

$$W_{a\to b} = \frac{2\pi}{\hbar^2}|H'_{ab}(0)|^2 \sum_{\mathbf{v}} \sum_{\mathbf{u}} P_{a\mathbf{v}} |\langle \Theta_{a\mathbf{v}}|\Theta_{b\mathbf{u}}\rangle|^2 D(\omega_{b\mathbf{u},a\mathbf{v}}), \tag{4.4}$$

$$W_{b\to a} = \frac{2\pi}{\hbar^2}|H'_{ab}(0)|^2 \sum_{\mathbf{v}} \sum_{\mathbf{u}} P_{a\mathbf{u}} |\langle \Theta_{a\mathbf{v}}|\Theta_{b\mathbf{u}}\rangle|^2 D(\omega_{b\mathbf{u},a\mathbf{v}}), \tag{4.5}$$

where $P_{a\mathbf{v}}$ and $P_{b\mathbf{u}}$ denote the Boltzmann distribution,

$$D(\omega_{b\mathbf{u},a\mathbf{v}}) = \frac{1}{\pi}\frac{\gamma_{b\mathbf{u},a\mathbf{v}}}{\gamma^2_{b\mathbf{u},a\mathbf{v}} + \omega^2_{b\mathbf{u},a\mathbf{v}}} \tag{4.6}$$

and $|\langle \Theta_{a\mathbf{v}}|\Theta_{b\mathbf{u}}\rangle|^2$ is the Franck-Condon factor (FCF). As $\gamma_{b\mathbf{u},a\mathbf{v}} \to 0$, $D(\omega_{b\mathbf{u},a\mathbf{v}})$ reduces to the delta function, $\delta(\omega_{bu,av})$.

To evaluate the rate constants it is necessary to know the potential surfaces of the electronic states a and b. For this purpose, the harmonic surfaces are commonly used,

$$U_a(\mathbf{Q}) = E_a + \sum_j \frac{1}{2}\omega_j^2 Q_j^2, \quad U_b(\mathbf{Q}') = E_b + \sum_j \frac{1}{2}\omega_j'^2 Q_j'^2. \tag{4.7}$$

Only the single-vibronic-level rate constants for the displaced surfaces will be given in the following; a more general case is presented in Appendix B. Notice that using the integral representation for the Lorentzian and

$$\Theta_{a\mathbf{v}} = \prod_j \chi_{av_j}(Q_j), \quad \Theta_{b\mathbf{u}} = \prod_j \chi_{bu_j}(Q'_j), \tag{4.8}$$

Eq. (4.3) can be written as

$$W_{a\mathbf{v}} = \frac{1}{\hbar^2}|H'_{ab}(\mathbf{0})|^2 \int_{-\infty}^{\infty} dt e^{it\omega_{ba} - \gamma_{ba}|t|} \prod_j G_{v_j}(t), \tag{4.9}$$

where

$$G_{v_j}(t) = \sum_{u_j} |\langle \chi_{av_j}|\chi_{bu_j}\rangle|^2 \times \exp\left[it\left\{\left(u_j + \tfrac{1}{2}\right)\omega_j - \left(v_j + \tfrac{1}{2}\right)\omega_j\right\}\right]. \tag{4.10}$$

The time-correlation function $G_{v_j}(t)$ can be expressed as

$$G_{v_j}(t) = G_{0_j}(t) \sum_{m_j=0}^{v_j} \frac{v_j!\,[S_j(e^{it\omega_j/2} - e^{-it\omega_j/2})^2]^{v_j - m_j}}{m_j!\,[(v_j - m_j)!]^2}, \tag{4.11}$$

where S_j denotes the Huang-Rhys factor of the jth mode, $S_j = \omega_j \Delta Q_j^2/2\hbar$, and

$$G_{0_j}(t) = \exp[-S_j(1 - e^{it\omega_j})]. \tag{4.12}$$

In this case for $W_{a\mathbf{v}}$ we find

$$W_{a\mathbf{v}} = \frac{|H'_{ab}(0)|^2}{\hbar^2} \int_{-\infty}^{\infty} dt e^{i\omega_{ba} - \gamma_{ba}|t| - \Sigma_j S_j(1 - e^{it\omega_j})} \times \prod_j \left[\sum_{m_j}^{v_j} \frac{v_j!\{S_j(e^{it\omega_j/2} - e^{-it\omega_j/2})^2\}^{v_j - m_j}}{m_j!\{(v_j - m_j)!\}^2}\right]. \tag{4.13}$$

Since the interfacial ET process is faster than the vibrational relaxation, we need the transition rate from a single molecular vibronic level to the conduction band (or local states coupled to the adsorbed molecule) of the solid surface. Formally, if the initial vibronic state of the adsorbent is labeled by the electronic level i and the vibrational level $\mathbf{v}$ (there are generally more than one vibrational mode), then the single-level ET rate constant is

$$W_{i\mathbf{v}} = \frac{|H'_{fi}|^2}{\hbar^2} \int_{-\infty}^{\infty} dt \exp\left[-\sum_k S_k(1 - e^{it\omega_k}) + it\omega_{fi} - \gamma_{if}|t|\right] \times \sum_{\mathbf{n}}^{\mathbf{v}} \prod_\ell \frac{v_\ell!}{(v_\ell - n_\ell)!(n_\ell!)^2}[S_\ell(e^{it\omega_\ell/2} - e^{-it\omega_\ell/2})^2]^{n_\ell}, \tag{4.14}$$

where v_ℓ denotes the vibrational state prepared by the pumping laser. Since the final electronic state f is related to the conduction band (or local states coupled to the adsorbed molecule) of the acceptor, a summation over f is required, and since the conduction band (or local states) is considered as a continuum, the summation will be rewritten into an integral,

$$\sum_f \to \int g(E)dE, \tag{4.15}$$

where $g(E)$ denotes the density of states

$$g(E) = \sum_f \delta(E - E_f). \tag{4.16}$$

If $g(E)$ takes the Gaussian form, then $W_{i\mathbf{v}}$ becomes

$$W_{i\mathbf{v}} = \frac{|H'_{fi}|^2}{\hbar^2} \int_{-\infty}^{\infty} dt \exp\left[-\sum_k S_k(1 - e^{it\omega_k}) + it\bar{\omega}_{fi} - \frac{D^2t^2}{4}\right] \times \sum_{\mathbf{n}}^{\mathbf{v}} \prod_\ell \frac{v_\ell!}{(v_\ell - n_\ell)!(n_\ell!)^2}[S_\ell(e^{it\omega_\ell/2} - e^{-it\omega_\ell/2})^2]^{n_\ell}, \tag{4.17}$$

where D represents the width in the Gaussian band shape. The average energy gap $\bar{\omega}_{fi}$ used here in the place of the energy gap is the difference between the photoexcited state energy and the center of the density of final states function, that is, the center of the Gaussian band shape in the present case. In this case, $g(E)$ plays the role of inhomogeneities. Although in principle, depending on the pumping laser pulse more than one vibrational mode can be excited, in most cases only one mode is involved in $W_{i\mathbf{v}}$, i.e.,

$$W_{i\mathbf{v}} = \frac{|H'_{fi}|^2}{\hbar^2} \int_{-\infty}^{\infty} dt \exp\left[-\sum_k S_k(1 - e^{it\omega_k}) + it\bar{\omega}_{fi} - \frac{D^2t^2}{4}\right] \times \sum_{n_\ell}^{v_\ell} \frac{v_\ell!}{(v_\ell - n_\ell)!(n_\ell!)^2}[S_\ell(e^{it\omega_\ell/2} - e^{-it\omega_\ell/2})^2]^{n_\ell}. \tag{4.18}$$

In a previous paper,[14] we have shown that in the strong coupling case (i.e., $\Sigma_\ell S_\ell \gg 1$), for the thermal average rate constant, in the classical regime the Marcus equation can be

TABLE I. The parameters of the vibrational modes used in the fitting of the absorption spectra of DTB-Pe molecule in toluene solution and on TiO_2 surface. The S value is the Huang-Rhys factor, or the (vibronic) coupling constant.

Mode	1	2	3	4	5	6	7	Inhomogeneity (d/cm^{-1})
Frequency (cm^{-1})	3000	1500	530	420	360	275	30	
S (in toluene)	0.05	0.72	0.3	0.2	0.2	0.2	2.5	250
S (on TiO_2)	0.05	1.0	0.3	0.2	0.2	0.2	3.0	450

derived by using the harmonic displaced surfaces. It has been shown that the reaction coordinate is well defined only in the Marcus theory, that is, in the classical regime. In this case, the reaction coordinate is along the minimum crossing point in the multidimensional potential surfaces (i.e., multimode case). In the quantum regime, the reaction coordinate is not well defined especially in the case of the nonrelaxed ET such as W_{iv}.

For a system in which more than one vibrational state is pumped at the same time, the population decay (into the product state and heat) dynamics can be described by the initial-population-weighted average of the single-level ET rates. However, the transient oscillation in population in short time after pumping cannot be represented by the rate process. Moreover, to calculate the quantum beat, even the oscillation in population is not enough. Coherence parts have to be included to completely model the spectroscopic signals. Finally, if we also want to study the dynamics of the product state, single-initial-level rate is not good enough, for the product vibrational levels are summed over. We need to calculate the state-to-state dynamics between the reactant and product electronic states.

V. APPLICATIONS AND DISCUSSION

To show the applications of the theoretical results presented in the previous sections, we shall use the DTB-Pe/TiO_2 system as an example.[11] DTB-Pe (2,5-di-*tert*-butyl-9-perylenyl-methyl-phosphonic acid) is a derivative of perylene in which the perylenyl group works as the chromophore and there are side groups for preventing the formation of chromophore complex, as well as linker group for chemisorbtion on TiO_2 surface. Recently Zimmermann *et al.*[11] have employed the 20 fs laser pulses to study the ET dynamics in the DTB-Pe/TiO_2 system and for comparison, they have also studied the excited state dynamics of free perylene in toluene solution. Limited by the 20 fs pulse duration, from the uncertainty principle, they can only observe the vibrational coherences (i.e., vibrational wave packets) of low frequency modes. Six significant modes, 275, 360, 420, 460, 500, and 625 cm^{-1}, have been resolved from the Fourier transform spectra of ultrashort pulse measurements. For detail of the analysis of the quantum beat, refer to Figs. 5–7 of Zimmermann *et al.*[11] These modes should play an important role not only in ET dynamics or excited state dynamics but also in absorption spectra. Therefore, we fit the steady-state absorption spectra of DTB-Pe, both in toluene solution and on TiO_2 surface, to determine the properties of these vibrational modes. To reduce the number of parameters in the model, however, we group the modes of 460, 500, and 625 cm^{-1} which are comparatively weak in the quantum beat amplitude into one average mode of frequency 530 cm^{-1}. From the vibronic structures of absorption spectra we obtain two additional modes, 1500 and 3000 cm^{-1}. Notice that these two modes cannot be observed in the quantum beat in this experiment. Using these modes with their corresponding Huang-Rhys factors shown in Table I, we reconstruct the absorption spectra of perylene-toluene solution and the perylene-TiO_2 system [see Figs. 4(a) and 4(b)]. The experimental absorption spectra are obtained from those published by Zimmermann *et al.* in the aforementioned paper.

The expression of the absorption coefficient from the initial electronic level a to upper electronic level b in the multidisplaced-mode case is[14]

$$\alpha(\omega) = \frac{2\pi|\boldsymbol{\mu}_{ba}|^2\omega}{3\hbar c}\int_{-\infty}^{\infty} dt \exp\left\{ it(\bar{\omega}_{ba} - \omega) - \frac{d^2t^2}{4} - \sum_j S_j[1 + 2\bar{n}_j - \bar{n}_j e^{-it\omega_j} - (1 + \bar{n}_j)e^{it\omega_j}]\right\}, \quad (5.1)$$

where d describes the width of inhomogeneity distribution and c is the light speed in vacuum. The 0-0 transition energy $\bar{\omega}_{ba}$ is 22 070 cm^{-1} in the solution and 21 950 cm^{-1} on TiO_2

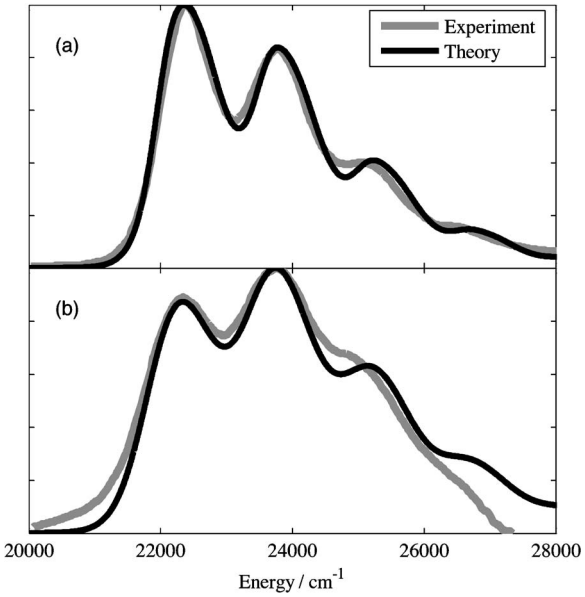

FIG. 4. Experimentally observed absorption spectra of DTB-Pe molecule (blue line) and the theoretical fitting (black line) with parameters given in Table I. (a) The result in toluene and (b) the result of DTB-Pe on TiO_2 surface. The 0-0 transition energies are is 22 070 cm^{-1} in the toluene solution and 21 950 cm^{-1} on TiO_2 surface.

surface. The agreement between experimental and calculated spectra is quite reasonable. Note that for the purpose of fitting, we also included a 30 cm^{-1} mode which plays the effect of all possible low-frequency modes. This 30 cm^{-1} mode is not considered in the computations of ET rates. Recently Wang *et al.* also analyzed the absorption spectra of a series of DTB-Pe dyes in solution and on TiO_2 surface with different linker groups.[24] To fit the spectra they introduce a single-vibrational-mode model with only a 1370 cm^{-1} mode which is assigned to a perylene in-plane C–C stretching mode. In our work, we also include those vibrational modes below 600 cm^{-1} that are involved in the quantum beat. The effect of the 1370 cm^{-1} mode introduced by Wang *et al.* has a large displacement and it has a similar effect on the fitting as the strong-coupling mode 1500 cm^{-1} we use here.

The role of the inhomogeneity d is also important. The effect of the inhomogeneity term is subtly different from other effects such as the strong-coupling low-frequency modes. The values of 250 and 450 cm^{-1} we use here for DTB-Pe in solution and DTB-Pe/TiO_2, respectively, were obtained with little ambiguity in the fitting. Therefore we believe that the increase of d by 200 cm^{-1} from the solution case to the adsorbed case reflects the real order of magnitude of the increase in inhomogeneity on the surface. Such an increase of inhomogeneity, as well as the shift of the absorption band origins, can usually be related to the interaction between the chromophore and the surface. In other words, our fitting indicates that the coupling between the photoexcited state (which is the initial state of the PIET process) and the surface is between 100 and 200 cm^{-1}.

In summary, some information concerning the properties of the vibrational modes relevant to the PIET process as well as the interaction of the dye molecule with the TiO_2 surface is revealed through the fitting of the absorption spectra.

To simulate the ET process in the DTB-Pe/TiO_2 system, however, we need to know the vibrational modes which can be divided into pumping modes and accepting modes. In addition to the eight modes obtained from the analysis of absorption spectra, there may be some high-frequency accepting modes participating in ET, but the Huang-Rhys factors for these high-frequency modes are usually very small and thus these modes will not be included in our ET rate calculations. In the DTB-Pe/TiO_2 case, even though the initial excited electronic state is well defined, the final charge-transfer state and its density of state distribution are unclear. In this work we use a Gaussian distribution of density of states to represent the final state. Other functional form of the density of states such as

$$g(E) = \frac{\sqrt{E}}{2\pi^2}\left(\frac{2m^*}{\hbar}\right)^{3/2} \tag{5.2}$$

has been used by Anderson and Lian.[10]

It should be noted that the ultrafast PIET is usually studied by the pump-probe experiment using ultrashort laser pulses. The probe signals usually include the dynamical information of both coherence and population and to obtain the PIET rate, a theoretical analysis of these signals is required. This has been accomplished for the studies of ultrafast PIET in bacterial photosynthetic reaction centers.[14]

TABLE II. The energy gaps of the transitions.

Transition	$S_1 \leftarrow g$	$S_n \leftarrow S_1$	$CT_n \leftarrow CT_1$
Energy gap (cm^{-1})	24 850	14 000	17 250

Next we shall present the model calculation of the PIET dynamics as observed through transient spectra. In this process, five different electronic levels are involved, each having a specific potential energy curve. These levels are the ground electronic state g, the directly photoexcited state S_1 (the initial state of the ET reaction) which is assumed to be neutral, the neutral higher excited electronic level S_n which is the final state of the induced absorption from S_1, the charge-separated state CT_1 which is the final state of the ET reaction, and the higher excited charge-separated electronic level CT_n which is the final state of the induced absorption from CT_1. Therefore, numerous parameters are involved in the model. Some of the parameters, such as the potential energy surfaces of g and S_1, were determined through fitting the steady-state spectra. Most of the other parameters are unknown due to the lack of experimental characterization and theoretical studies. We choose to demonstrate the typical behavior of a PIET process by studying a one-vibrational mode system instead of using a multimode model as that used in fitting the absorption spectra. Hopefully the effect of each parameter will be clearer in the result for us to gain qualitative understanding of the beating phenomenon.

In the calculations, we assume that the pumping laser only excites the system from the ground state to the first two vibrational levels of the S_1 state. These two levels are coherently excited. Then we integrate the Liouville equation of the system to obtain the time dependence of the population of the S_1 and CT_1 levels, the coherence within respective levels, and the coherence between them. For each moment of time, we use the band shape functions of transition between S_1 and S_n and between CT_1 and CT_n together with the density matrix elements of each electronic levels to calculate the susceptibility $\chi(\omega,t)$, whose imaginary part is proportional to the absorption spectra. The relative energies of the electronic levels in our calculation are listed in Table II. The energy gaps between S_n and S_1 and that between CT_n and CT_1 only affect the position of the induced spectral features. The energy gap between S_1 and CT_1, instead, strongly influences the PIET dynamics. Therefore, it is changed in the calculation and will be discussed later.

First, we use one vibrational mode with frequency 420 cm^{-1} in the calculation. The coupling constants between different electronic potential energy surfaces are given in Table III. Most of the couplings are very weak. The coupling

TABLE III. The coupling constant S between different electronic potential surfaces and the inhomogeneity D in calculating the transient absorption spectra.

Transition	$S_1 \leftarrow g$	$CT_1 \leftarrow S_1$	$S_n \leftarrow S_1$	$CT_n \leftarrow CT_1$
Coupling const.	0.3	0.5	0.05	1
Inhomogeneity			450 cm^{-1}	1300 cm^{-1}

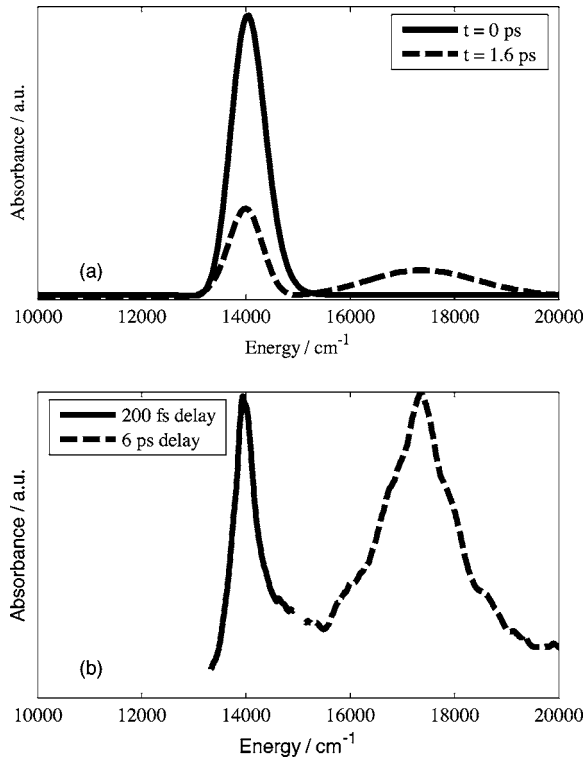

FIG. 5. (a) The induced absorption spectra constructed from the theory. At time $t=0$, the induced absorption is from the reactant state to higher neutral states S_n, while at time $t=1.6$ ps, contributions from both reactant state and product state appear. (b) In the work of Burfeindt *et al.* (Ref. 25), the induced absorption at $t=200$ fs is attributed to the reactant induced absorption, while at $t=6$ ps they conclude that the induced absorption from the product state is observed.

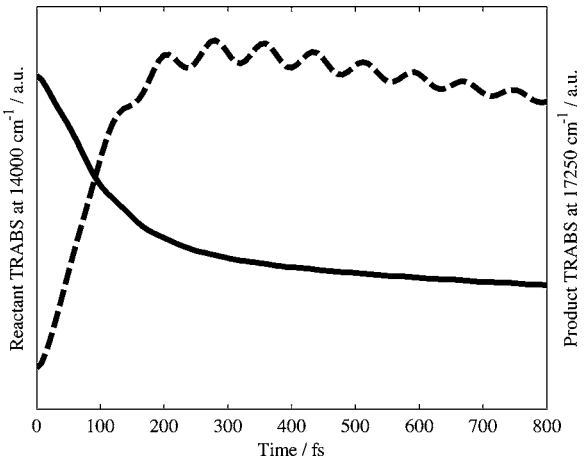

FIG. 6. The theoretical calculation of the time trace of transient absorption (TRABS) for a one-mode system. The energy gap is 20 cm^{-1} and the vibrational mode is 420 cm^{-1}. The solid curve is the reactant TRABS, and the dashed curve is the product TRABS. The probing frequency is set at respective peak positions of the induced absorption spectra of both reactant and product states. For discussion see text.

between the CT_n surface and CT_1 is larger but it only influences the line shape of the induced absorption from CT_1. We choose weak coupling constants, first, in accordance with the characteristics of the absorption spectra and second, to make the trend of the demonstrative calculations simpler. Indeed, strong coupling cases present more sophisticated dynamics, and those phenomena are too complicated to be discussed in the length of the present article. It shall be left to be discussed in later articles focusing on specific systems. Besides, later we shall also change the frequency of the vibrational mode, but we shall keep these parameters of the potential energy surfaces constant for simplicity.

We mentioned that we assume that initially only the lowest two vibrational states in the S_1 level are excited. This is equivalent to saying that we fixed the pumping energy just above the 0-0 transition from ground state to S_1. In the calculation, we only assume that there is a single final state of ET reaction (CT_1). We compute the density matrix elements of this state, construct the induced absorption from it to one CT_n state, and then assume that there is a large inhomogeneity in this level so that we convolute a Gaussian inhomogeneity with the calculated spectra. By doing this we implicitly assume several things. First, we assume that the inhomogeneity at least partly reflects the width of the distribution of the final density of state. More importantly, in this approach we assume that the electronic coupling between S_1 and all of these final states is constant. Whether or not this assumption is reasonable has to be examined by detailed studies of the properties of the electronic states of the adsorption system, either through quantum chemistry calculations or by further experiments. Here we assume that the molecular orbitals of the chromophore are weakly overlapping with the atomic orbitals of the surface so that the electronic coupling is only determined by the interaction Hamiltonian matrix elements between the molecular orbitals of the charge-separated state and the photoexcited state of the adsorbent. Second, by doing so we also assume that intraband transition in the conduction band of TiO_2 nanoparticle can be ignored in the time scale of our study. That is, for each electronic state inside the distribution of the final states, its density matrix elements of the vibrational states evolve with time independently of the density matrix elements of any other electronic states also inside the final state distribution. In other words, the population and coherence are not transferred between different final states of ET.

Now we discuss the results of the calculation. First, we show the calculation of the transient absorption spectra in the range of 10 000–20 000 cm^{-1} right after pumping (time delay equals 0 ps) and 1.6 ps after pumping. The result is plotted in Fig. 5(a). The energy gap between the CT_1 state (will be named the state b afterwards for brevity) and S_1 state (will be written as state a afterwards), ω_{ba}, is 20 cm^{-1}, that is, nearly resonant. The ET reaction is efficient despite the weak coupling because of this small energy gap. At time zero, the transient absorption comes from level a, while after 1.6 ps there are obvious absorptions from both the reactant state a and the product state b. To get a feeling of how this approximately reproduces the trend of the experiments, we show in Fig. 5(b) the transient absorption spectra of DTB-Pe on TiO_2 surface at 200 fs and 6 ps after pumping, observed by Burfeindt *et al.*[25]

Experimentally, the transient absorption is observed by measuring the intensity of a probe laser pulse. The observed dynamics is related to the frequency of this pulse (see Sec. II). For brevity we refer to the central frequency of the line shape of the probe pulse as the probing frequency. However,

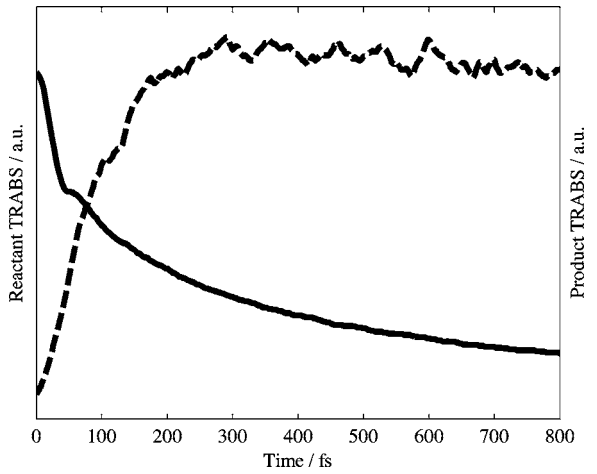

FIG. 7. The experimental observation of the reactant TRABS and product TRABS, done by Zimmermann *et al.* (Ref. 11). For discussion see text.

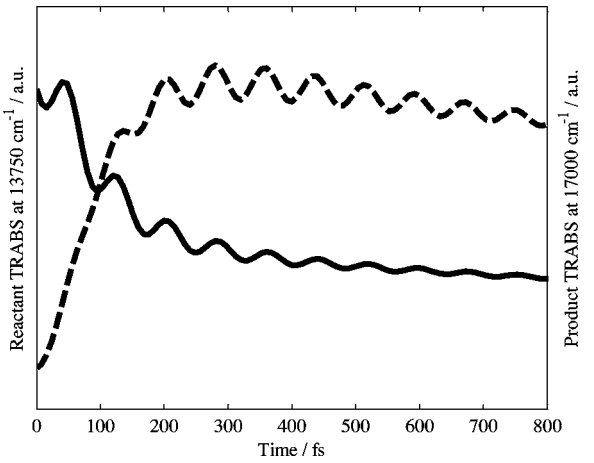

FIG. 9. The TRABS dynamics observed at 250 cm^{-1} to the red side of the respective peak positions of the induced absorption spectra of both reactant and product state. For discussion see text.

presently we do not consider the shape of the probe pulse. We only calculate the transient absorption at the probing frequency to simulate the probing signal. The result of the simulation on the above model system, probed at the respective peak position of the induced absorption of both the reactant and the product states, is shown in Fig. 6. Notice that in our simulation the electronic coupling value is 70 cm^{-1} and the ET dynamics is almost as fast as experimentally observed. The experimental result by Zimmermann *et al.* is shown in Fig. 7.

For comparison, we show the same calculation, but change the vibrational frequency to 275 cm^{-1} in Fig. 8. The feature of the dynamics is almost similar, except that the period of the quantum beat is longer. Therefore, hereafter we shall focus only on the results for the 420 cm^{-1} mode.

Next we show the transient absorption observed at other positions. Experimentally, the observations are not always made at the peak positions. In Fig. 9, the probing frequencies are moved 250 cm^{-1} to the red, that is, to 13 750 and 17 000 cm^{-1}, respectively. The quantum beats of transient absorption in both the reactant and the product states become more pronounced. It can be shown that according to our calculations the quantum beats are more pronounced when the probing frequencies are shifted to either side of the peaks, at least for shifts smaller than 250 cm^{-1}.

The next phenomenon we discuss here is the energy-gap dependence. To demonstrate this effect, we fix our observation at the peak positions of the induced absorptions to reduce complications from the stronger quantum beats. In Fig. 10 we show the case when the energy gap is increased to 200 cm^{-1}. The ET dynamics is less efficient than the case of the 20 cm^{-1} gap. This is reasonable because in the case of single displaced mode, the smaller the energy gap, the better the resonance between the initial and final vibronic levels. In the weak coupling case, the Franck-Condon overlap integral is the largest between $v=0$ states of initial and final electronic levels. We can expect that if the pumping energy is close to the bottom of the reactant state so that the $v=0$ level is efficiently excited, and if at the same time the energy gap between the reactant and product electronic levels is small, the ET reaction will be much faster than in other conditions. It is possible that this is the condition satisfied by most of the dye/semiconductor systems having high PIET efficiency. For

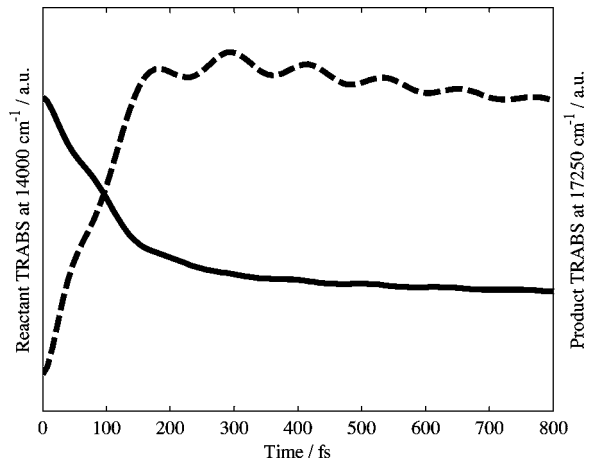

FIG. 8. TRABS time trace constructed theoretically for the one-mode model system. Here the frequency of the mode is changed to 275 cm^{-1}. For discussion see text.

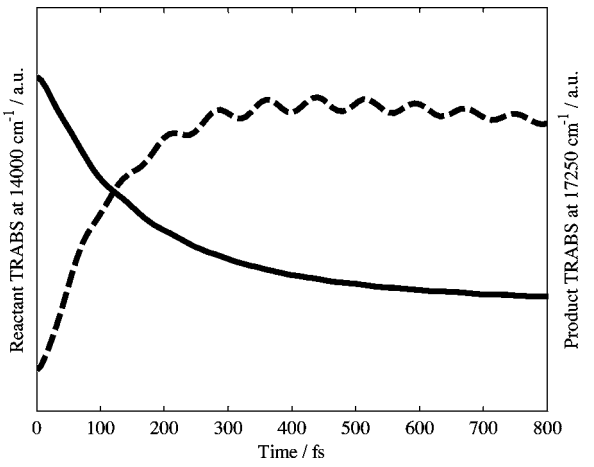

FIG. 10. The TRABS dynamics of the model system when the energy gap between reactant and product is increased to 200 cm^{-1}. The other conditions are the same as in Fig. 6. For discussion see text.

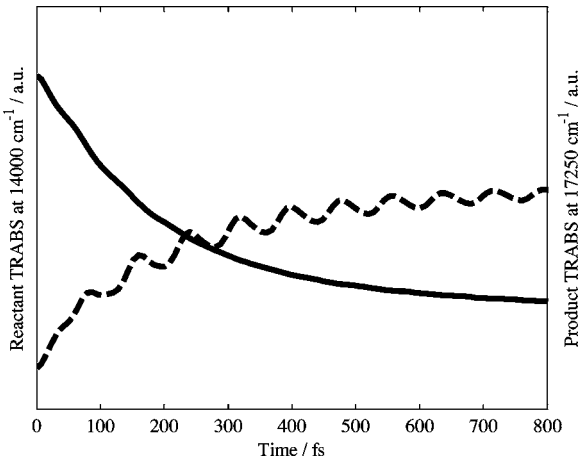

FIG. 11. The TRABS dynamics of the model system when the energy gap between reactant and product is increased to 420 cm^{-1}. The other conditions are the same as in Fig. 6. For discussion see text.

a pair of one-dimensional displacement-only potential energy surfaces, the wave function of the ground vibrational level of the reactant state, for example, has the greatest overlap with a vibrational level in the product state whose quantum number is closest to the Huang-Rhys factor. In other words, the ET rate is the highest when the energy gap is around $S\hbar\omega$. Thus, when the vibronic coupling is strong, the optimal band gap value may be large. However, since in this case the Franck-Condon factor between the $v=0$ vibrational level of the reactant electronic state and the $v=n$ vibrational level of the product electronic state is $F_{0n} \sim e^{-S}S^n/n!$, obviously even when the energy gap value is close to the optimal value, the small FC factor value still makes the ET rate much smaller than in the small band gap case with weak vibronic coupling, if the electronic coupling is the same. To design a better system for solar cell, it is desirable to achieve suitable conditions that can enhance ET. This may be one of the directions to consider. On the other hand, one may question how the product state may be close to the reactant state in energy. This has to be studied by more sophisticated experiments that can determine the energy of the product state, or by high-level quantum chemistry computations. Here we only make the comment that, even if the isolated dye molecule (or in solution) may have a relative larger energy gap between these two states, the interaction between the dye with the solid surface may shift the charge-separated state significantly. This is already well understood in the case of hydrogen adsorption to metal surface.[26] Since resonance condition is even stronger than the contribution from Franck-Condon factor, it is indeed interesting to study whether we can discover systems with nearly resonant reactant and product electronic states. The other problems limiting the efficiency in dye-sensitized solar cells, such as the back electron transfer, may be tackled with other methods.[27] Finally, in Fig. 11 we show the case when the energy gap is increased to 420 cm^{-1}. When all of the other conditions are kept the same, it is seen that the ET dynamics is obviously slowed down. Notice that in this case the initially prepared vibronic states, that is, the $v=0$ and $v=1$ states of the initial electronic level, are resonant to the $v=1$ and $v=2$ states of the final electronic levels, respectively, but the ET efficiency still decreases.

In this paper we have employed the golden rule to study ET; for numerical demonstrations we have chosen the DTB-Pe/TiO_2 system and used the magnitude of 70 cm^{-1} for the electronic coupling matrix element which leads to the ET rate in the time scale of 100–200 fs. The validity and applicability of the golden rule depend on the magnitude of electronic coupling matrix element, electronic energy gap, Franck-Condon factor, density of state, and dephasing rate (or damping). We have checked the effect of higher order approximation and found that the golden rule is applicable under the conditions used in this paper. It should be noted that the golden rule expression given by Eqs. (4.1)–(4.5) describes the so-called direct ET or ET through space. High-order approximations for calculating ET rate can be investigated by using the Green's function method[28] and density matrix method.[29] For the case in which there exists no resonant intermediate electronic state between the initial excited electronic state and the final charge-transfer state, ET can take place through space and also via superexchange (or through bonds), and the Marcus type of ET expression can be obtained in this case. On the other hand, for the case in which there exists a resonant intermediate electronic state, the distance dependence and temperature dependence of ET become very complicated. Furthermore, sequential ET can also take place in competition.

From the magnitude of the computed single-level ET rate and the value of electronic coupling chosen for the computation (70 cm^{-1}), it is seen that to achieve ET rate faster than 100 fs, it is not necessary to have a strong electronic coupling. Rather, the properties of the final state of the ET process are also important factors.

To help us completely understand the ultrafast interface ET between dye molecules and semiconductor nanoparticles, it is desirable to experimentally measure the femtosecond time-resolved spectra (i.e., probing signal in the pump-probe experiment) at various pumping wavelengths. Changing laser pulse durations will also be useful.

In concluding this paper, it is desirable to theoretically perform quantum chemistry calculation to study the interactions between adsorbed dye molecule and semiconductor in order to determine the exact location of the charge-transfer state, the final density of states distribution, and the effect of local defects caused by the interaction between the dye molecule and the semiconductor and to obtain the potential surfaces involved in excitation and ET including the interactions between these surfaces. Although Marcus and co-workers[30,31] have performed the tight-binding calculations for the Si/viologen and InP/Me_2Fe systems, higher-level calculations are desirable.

ACKNOWLEDGMENT

This work is financially supported by the National Science Council of Taiwan and Academia Sinica, Taiwan.

APPENDIX A: DERIVATION OF THE TCF FOR THE BAND-SHAPE FUNCTION

We continue the derivation starting from Eq. (2.21). Defining the new variables $\lambda_j=-\omega_j t$, $\mu_j'=\omega_j' t$, the time-correlation function $G_{av_j',av_j}(t)$ is further written as follows:

$$G_{av_j',av_j}(t)=e^{-i(v_j+1/2)\lambda_j}\sum_{u_j}e^{-i(u_j+1/2)\mu_j'}\langle\chi_{av_j'}|\chi_{bu_j}\rangle\langle\chi_{bu_j}|\chi_{av_j}\rangle. \tag{A1}$$

By using the Mehler's formula in the sinusoidal-function form,

$$G_{av_j',av_j}(t)=e^{-i(v_j+1/2)\lambda_j}(-1+i)\sqrt{\frac{\beta_j'}{4\pi\sin\mu_j'}}\int_{-\infty}^{\infty}\int_{-\infty}^{\infty}dQ_j d\bar{Q}_j\chi_{av_j}(Q_j)\chi_{av_j'}(\bar{Q}_j)e^{-i\beta_j'/4[(Q_j'+\bar{Q}_j')^2\tan\mu_j'/2-(Q_j'-\bar{Q}_j')^2\cot\mu_j'/2]}. \tag{A2}$$

Next, we shall consider the displaced-oscillator case, that is, $\omega_j'=\omega_j$, $\beta_j'=\beta_j$ and $\mu_j'=-\lambda_j$. By using the contour integral representation of the Hermite polynomials [see Eq. (B4)], we have

$$\begin{aligned}G_{av_j',av_j}(t)=&(-)^{v_j+v_j'}(-1+i)e^{-i(v_j+1/2)\lambda_j}\sqrt{\frac{\beta_j/\pi}{2^{v_j}v_j!2^{v_j'}v_j'!}}\sqrt{\frac{\beta_j}{4\pi\sin\mu_j'}}\\&\times\frac{v_j!v_j'!}{(2\pi i)^2}\oint\frac{dZ_1e^{-Z_1^2}}{Z_1^{v_j+1}}\oint\frac{dZ_2e^{-Z_2^2}}{Z_2^{v_j'+1}}\int\int dQ_j d\bar{Q}_j e^{-2Z_1\sqrt{\beta_j}Q_j-2Z_2\sqrt{\beta_j}\bar{Q}_j}\\&\times\exp\left\{-\frac{\beta_j}{4}\left[(Q_j+\bar{Q}_j)^2+(Q_j-\bar{Q}_j)^2+i(Q_j'+\bar{Q}_j')^2\tan\frac{\mu_j'}{2}-i(Q_j'-\bar{Q}_j')^2\cot\frac{\mu_j'}{2}\right]\right\},\end{aligned} \tag{A3}$$

where $\bar{Q}_j'=Q_j+d_j$ and $\bar{Q}_j'=\bar{Q}_j+d_j$, thus $Q_j'+\bar{Q}_j'=Q_j+\bar{Q}_j+2d_j$ and $Q_j'-\bar{Q}_j'=Q_j-\bar{Q}_j$. Letting $X=(Q_j+\bar{Q}_j)/\sqrt{2}$ and $Y=(Q_j-\bar{Q}_j)/\sqrt{2}$, we have $dQ_jd\bar{Q}_j=dXdY$ and

$$\begin{aligned}G_{av_j',av_j}(t)=&(-)^{v_j+v_j'}(-1+i)e^{-i(v_j+1/2)\lambda_j}\sqrt{\frac{v_j!v_j'!}{2^{v_j+v_j'+2}\pi^2\sin\mu_j'}}\\&\times\frac{\beta_j}{(2\pi i)^2}\oint\frac{dZ_1e^{-Z_1^2}}{Z_1^{v_j+1}}\oint\frac{dZ_2e^{-Z_2^2}}{Z_2^{v_j'+1}}\int\int dXdYe^{-\sqrt{2\beta_j}Z_1(X+Y)-\sqrt{2\beta_j}Z_2(X-Y)}\\&\times\exp\left\{-\frac{\beta_j}{2}\left[X^2+Y^2+i(X+\sqrt{2}d_j)^2\tan\frac{\mu_j'}{2}-iY^2\cot\frac{\mu_j'}{2}\right]\right\}.\end{aligned} \tag{A4}$$

The terms in the exponentials in the integrand can be simplified by observing that

$$\begin{aligned}&-\sqrt{2\beta_j}Z_1(X+Y)-\sqrt{2\beta_j}Z_2(X-Y)-\frac{\beta_j}{2}\left[X^2+Y^2+i(X+\sqrt{2}d_j)^2\tan\frac{\mu_j'}{2}-iY^2\cot\frac{\mu_j'}{2}\right]\\&=-\frac{\beta_j}{2}\left(1+i\tan\frac{\mu_j'}{2}\right)X^2-\sqrt{2\beta_j}\left(Z_1+Z_2+i\sqrt{\beta_j}d_j\tan\frac{\mu_j'}{2}\right)X\\&\quad-\frac{\beta_j}{2}\left(1-i\cot\frac{\mu_j'}{2}\right)Y^2-\sqrt{2\beta_j}(Z_1-Z_2)Y-i\beta_jd_j^2\tan\frac{\mu_j'}{2}.\end{aligned} \tag{A5}$$

Thus we can first carry out the integrals over Y and X,

$$\int_{-\infty}^{\infty}dYe^{-\beta_j/2(1-i\cot\mu_j'/2)Y^2-\sqrt{2\beta_j}(Z_1-Z_2)Y}=\sqrt{\frac{2\pi}{\beta_j(1-i\cot\mu_j'/2)}}\exp\left\{(Z_1-Z_2)^2\Big/\left(1-i\cot\frac{\mu_j'}{2}\right)\right\} \tag{A6}$$

and

$$\begin{aligned}&\int_{-\infty}^{\infty}dXe^{-\beta_j/2(1+i\tan\mu_j'/2)X^2-\sqrt{2\beta_j}(Z_1+Z_2+i\sqrt{\beta_j}d_j\tan\mu_j'/2)X}\\&=\sqrt{\frac{2\pi}{\beta_j(1+i\tan\mu_j'/2)}}\exp\left\{\left(Z_1+Z_2+i\sqrt{\beta_j}d_j\tan\frac{\mu_j'}{2}\right)^2\Big/\left(1+i\tan\frac{\mu_j'}{2}\right)\right\}.\end{aligned} \tag{A7}$$

Then the time-correlation function can be written as

$$G_{av_j',av_j}(t) = (-)^{v_j+v_j'} e^{-i(v_j+1/2)\lambda_j} \frac{-1+i}{(2\pi i)^2} e^{-i\beta_j d_j^2 \tan \mu_j'/2} \sqrt{\frac{v_j! v_j'!}{2^{v_j+v_j'} \sin \mu_j' (1+i\tan \mu_j'/2)(1-i\cot \mu_j'/2)}}$$
$$\times \oint \frac{dZ_1 e^{-z_1^2}}{Z_1^{v_j+1}} \oint \frac{dZ_2 e^{-Z_2^2}}{Z_2^{v_j'+1}} \exp\left\{ \frac{(Z_1+Z_2+i\sqrt{\beta_j} d_j \tan \mu_j'/2)^2}{1+i\tan \mu_j'/2} + \frac{(Z_1-Z_2)^2}{1-i\cot \mu_j'/2} \right\}, \tag{A8}$$

which can be simplified as

$$G_{av_j',av_j}(t) = (-)^{v_j+v_j'} e^{-iv_j\lambda_j} \sqrt{\frac{v_j! v_j'!}{2^{v_j+v_j'}}} e^{-S_j(1-e^{i\lambda_j})}$$
$$\times \frac{1}{(2\pi i)^2} \oint \frac{dZ_1}{Z_1^{v_j+1}} \oint \frac{dZ_2}{Z_2^{v_j'+1}}$$
$$\times \exp\{2e^{i\lambda_j} Z_1 Z_2 + \kappa_j (Z_1+Z_2)\}, \tag{A9}$$

where κ_j is defined in Eq. (2.23). Next we make the expansion

$$e^{2Z_1 Z_2 e^{i\lambda_j}} = \sum_{n_j=0}^{\infty} \frac{(2Z_1 Z_2 e^{i\lambda_j})^{n_j}}{n_j!} \tag{A10}$$

and carry out the contour integrals as follows:

$$\frac{1}{(2\pi i)^2} \oint \frac{dZ_1}{Z_1^{v_j+1}} \oint \frac{dZ_2}{Z_2^{v_j'+1}} \sum_{n_j=0}^{\infty} \frac{(2e^{i\lambda_j})^{n_j}}{n_j!} Z_1^{n_j} Z_2^{n_j} e^{\kappa_j Z_1} e^{\kappa_j Z_2}$$
$$= \sum_{n_j=0}^{\infty} \frac{(2e^{i\lambda_j})^{n_j}}{n_j!} \frac{1}{(2\pi i)^2} \oint \frac{dZ_1 e^{\kappa_j Z_1}}{Z_1^{v_j-n_j+1}} \oint \frac{dZ_2 e^{\kappa_j Z_2}}{Z_2^{v_j'-n_j+1}}$$
$$= \sum_{n_j=0}^{\min(v_j,v_j')} \frac{(2e^{i\lambda_j})^{n_j}}{n_j!} \frac{\kappa_j^{v_j-n_j}}{(v_j-n_j)!} \frac{\kappa_j^{v_j'-n_j}}{(v_j'-n_j)!}. \tag{A11}$$

The resulting Eq. (A9) can be rewritten into the form of Eq. (2.22). Notice that we also replace λ_j by $\omega_j t$ in the final representation.

APPENDIX B: $G_{v_j}(t)$ FOR DISPLACED-DISTORTED OSCILLATOR

In the present case, we shall write

$$G_{v_j}(t) = e^{\lambda_j(v_j+1/2)} \sum_{u_j'} e^{-\mu_j'(u_j'+1/2)} |\langle \chi_{av_j}(Q_j) | \chi_{bu_j'}(Q_j') \rangle|^2, \tag{B1}$$

where $\lambda_j = -it\omega_j$ and $\mu_j' = -it\omega_j'$. Using the Slater sum, Eq. (B1) can be written as

$$G_{v_j}(t) = \frac{\sqrt{\beta_j'} e^{\lambda_j(v_j+1/2)}}{\sqrt{2\pi \sinh \mu_j'}}$$
$$\times \int_{-\infty}^{\infty} \int_{-\infty}^{\infty} dQ_j d\bar{Q}_j \chi_{av_j}(Q_j) \chi_{av_j}(\bar{Q}_j)$$
$$\times \exp\left\{ -\frac{\beta_j'}{2} \left[(Q_j'+\bar{Q}_j')^2 \tanh \frac{\mu_j'}{2} + (Q_j'-\bar{Q}_j')^2 \coth \frac{\mu_j'}{2} \right] \right\}, \tag{B2}$$

where $\beta_j' = \omega_j'/\hbar$ and

$$\chi_{av_j}(Q_j) = N_{av_j} H_{v_j}(\sqrt{\beta_j} Q_j) e^{-\beta_j Q_j^2/2}. \tag{B3}$$

With the contour-integral representation of the Hermite polynomial,

$$H_n(z) = (-1)^n \frac{n!}{2\pi i} \oint \frac{e^{-Z^2-2zZ}}{Z^{n+1}} dZ, \tag{B4}$$

it follows that

$$G_{v_j}(t) = K_{v_j} \frac{\sqrt{\beta_j'} e^{\lambda_j(v_j+1/2)}}{\sqrt{2\pi \sinh \mu_j'}} \int_{-\infty}^{\infty} \int_{-\infty}^{\infty} dQ_j d\bar{Q}_j e^{-\beta_j'/4[(Q_j'+\bar{Q}_j')^2 \tanh \mu_j'/2 + (Q_j'-\bar{Q}_j')^2 \coth \mu_j'/2]} e^{-\beta_j(Q_j^2+\bar{Q}_j^2)/2} \oint \frac{dZ_1}{Z_1^{v_j+1}}$$
$$\times \oint \frac{dZ_2}{Z_2^{v_j+1}} e^{-(Z_1^2+Z_2^2)-2\sqrt{\beta_j}(Z_1 Q_j + Z_2 \bar{Q}_j)}, \tag{B5}$$

where $Q_j' = Q_j + d_j$ and

$$K_{v_j} = \left[\frac{(-1)^{v_j} v_j! N_{av_j}}{2\pi i} \right]^2. \tag{B6}$$

By using the new variables $X = (Q_j + \bar{Q}_j)/\sqrt{2}$ and $Y = (Q_j - \bar{Q}_j)/\sqrt{2}$, Eq. (B5) can be simplified as

$$G_{v_j}(t) = K_{v_j} \frac{\sqrt{\beta_j'} e^{\lambda_j(v_j+1/2)}}{\sqrt{2\pi \sinh \mu_j'}} \oint \frac{dZ_1}{Z_1^{v_j+1}} \oint \frac{dZ_2}{Z_2^{v_j+1}} e^{-(Z_1^2+Z_2^2)} I_X I_Y, \tag{B7}$$

where

$$I_X = \sqrt{\frac{2\pi}{\beta_j + \beta_j' \tanh \mu_j'/2}} \exp\left\{ - \frac{\beta_j \beta_j' \tanh(\mu_j'/2)}{\beta_j + \beta_j' \tanh(\mu_j'/2)} d_j^2 + \frac{\beta_j (Z_1 + Z_2)^2 + 2\sqrt{\beta_j}\beta_j' \tanh(\mu_j'/2) d_j (Z_1 + Z_2)}{\beta_j + \beta_j' \tanh(\mu_j'/2)} \right\} \tag{B8}$$

and

$$I_Y = \sqrt{\frac{2\pi}{\beta_j + \beta_j' \coth \mu_j'/2}} \exp\left\{ \frac{\beta_j (Z_1 - Z_2)^2}{\beta_j + \beta_j' \coth(\mu_j'/2)} \right\}. \tag{B9}$$

It follows that

$$G_{v_j}(t) = K_{v_j} \sqrt{\frac{2\pi\beta_j'}{(\beta_j^2 + \beta_j'^2)\sinh \mu_j' + 2\beta_j\beta_j' \cosh \mu_j'}} \exp\left\{ \lambda_j \left(v_j + \frac{1}{2} \right) - \frac{\beta_j' \sinh \mu_j'/2 (\sqrt{\beta_j} d_j)^2}{\beta_j \cosh \mu_j'/2 + \beta_j' \sinh \mu_j'/2} \right\} \oint \frac{dZ_1}{Z_1^{v_j+1}} \oint \frac{dZ_2}{Z_2^{v_j+1}}$$
$$\times \exp\left\{ - (Z_1^2 + Z_2^2) + \frac{\beta_j (Z_1 - Z_2)^2}{\beta_j + \beta_j' \coth \mu_j'/2} + \frac{\beta_j (Z_1 + Z_2)^2}{\beta_j + \beta_j' \tanh \mu_j'/2} + \frac{2\beta_j' \tanh \mu_j'/2 \sqrt{\beta_j} d_j (Z_1 + Z_2)}{\beta_j + \beta_j' \tanh \mu_j'/2} \right\} \tag{B10}$$

or

$$G_{v_j}(t) = \frac{F_{v_j}}{(2\pi i)^2} \oint \frac{dZ_1}{Z_1^{v_j+1}} \oint \frac{dZ_2}{Z_2^{v_j+1}} \exp\{ - A_j (Z_1^2 + Z_2^2) + B_j (Z_1 + Z_2) \} \exp\{ C_j Z_1 Z_2 \}, \tag{B11}$$

where for convenience we have introduced the following notations:

$$D_j = (\beta_j^2 + \beta_j'^2)\sinh \mu_j' + 2\beta_j\beta_j' \cosh \mu_j', \tag{B12}$$

$$E_j = (\beta_j'^2 - \beta_j^2)\sinh \mu_j', \tag{B13}$$

$$A_j = E_j / D_j, \tag{B14}$$

$$B_j = 2\beta_j' \sinh \frac{\mu_j'}{2} \sqrt{\beta_j} d_j \Bigg/ \left(\beta_j \cosh \frac{\mu_j'}{2} + \beta_j' \sinh \frac{\mu_j'}{2} \right), \tag{B15}$$

$$C_j = 4\beta_j\beta_j' / D_j, \tag{B16}$$

and

$$F_{v_j} = [(-1)^{v_j} v_j! N_{av_j}]^2 \sqrt{\frac{2\pi\beta_j'}{D_j}} \exp\left\{ - \frac{\beta_j' \sinh \mu_j'/2 (\sqrt{\beta_j} d_j)^2}{\beta_j \cosh \mu_j'/2 + \beta_j' \sinh \mu_j'/2} + \lambda_j (v_j + 1/2) \right\}. \tag{B17}$$

Then,

$$G_{v_j}(t) = \frac{F_{v_j}}{(2\pi i)^2} \sum_{n_j=0}^{\infty} \frac{C_j^{n_j}}{n_j!} \oint dZ_1 Z_1^{n_j - v_j - 1} e^{-A_j Z_1^2 + B_j Z_1} \oint dZ_2 Z_2^{n_j - v_j - 1} e^{-A_j Z_2^2 + B_j Z_2}$$
$$= F_{v_j} \sum_{n_j=0}^{v_j} \frac{C_j^{n_j}}{n_j!} \left[\frac{1}{2\pi i} \oint \frac{dZ}{Z^{v_j - n_j + 1}} e^{-A_j Z^2 + B_j Z} \right]^2$$
$$= F_{v_j} \sum_{n_j=0}^{v_j} \frac{C_j^{n_j} A_j^{v_j - n_j}}{n_j! [(v_j - n_j)!]^2} \left[\frac{(-1)^{v_j - n_j} (v_j - n_j)!}{2\pi i} \oint \frac{dz}{z^{v_j - n_j + 1}} e^{-z^2 - 2(B_j / 2\sqrt{A_j}) z} \right]^2$$
$$= F_{v_j} \sum_{n_j=0}^{v_j} \frac{C_j^{n_j} A_j^{v_j - n_j}}{n_j! [(v_j - n_j)!]^2} \left[H_{v_j - n_j} \left(\frac{B_j}{2\sqrt{A_j}} \right) \right]^2. \tag{B18}$$

In particular, if $d_j = 0$, then $B_j = 0$ and

$$G_{v_j}(t) = F_{v_j}(t) \sum_{n_j=0}^{v_j} \frac{C_j^{n_j} A_j^{v_j - n_j}}{n_j! [(v_j - n_j)!]^2} \left[\frac{(v_j - n_j)!}{\ell_j!} \delta_{2\ell_j, v_j - n_j} \right]^2 = F_{v_j}(t) \sum_{n_j=0}^{v_j} \frac{C_j^{n_j} A_j^{v_j - n_j}}{n_j!} \left[\frac{\delta_{2\ell_j, v_j - n_j}}{\ell_j!} \right]^2, \tag{B19}$$

where $\delta_{2\ell_j,v_j-n_j}$ denotes the Kronecker delta function. For example, we have

$$G_{0_j}(t) = F_{0_j}(t), \tag{B20}$$

$$G_{1_j}(t) = F_{1_j}(t)C_j, \tag{B21}$$

$$G_{2_j}(t) = F_{2_j}(t)\left(A_j^2 + \frac{1}{2!}C_j^2\right), \tag{B22}$$

$$G_{3_j}(t) = F_{3_j}(t)\left(C_jA_j^2 + \frac{1}{3!}C_j^3\right), \tag{B23}$$

and so on. Equation (4.11) can be obtained from Eq. (B18) by setting $\omega_j = \omega_j'$ and $d_j \neq 0$.

[1] A. Hagfeldt and M. Grätzel, Chem. Rev. (Washington, D.C.) **95**, 49 (1995).
[2] N. Anderson and T. Lian, Coord. Chem. Rev. **248**, 1231 (2004).
[3] A. Furube, R. Katoh, T. Yoshihara, K. Hara, S. Murata, H. Arakawa, and M. Tachiya, J. Phys. Chem. B **108**, 12583 (2004).
[4] K. Sebastian and M. Tachiya, J. Chem. Phys. **124**, 064713 (2006).
[5] A. Nitzan and M. A. Ratner, Science **300**, 1384 (2003).
[6] D. M. Adams, L. Brus, C. E. D. Chidsey *et al.*, J. Phys. Chem. B **107**, 6668 (2003).
[7] B. O'Regan, J. Moser, M. Anderson, and M. Grätzel, J. Phys. Chem. **94**, 8720 (1990).
[8] M. K. Nazeeruddin, A. K. Rodicio, R. Humphry-Baker, E. Müller, P. Liska, N. Vlachopoulos, and M. Grätzel, J. Am. Chem. Soc. **115**, 6382 (1993).
[9] D. F. Watson and G. J. Meyer, Annu. Rev. Phys. Chem. **56**, 119 (2005).
[10] N. A. Anderson and T. Lian, Annu. Rev. Phys. Chem. **56**, 491 (2005).
[11] C. Zimmermann, F. Willig, S. Ramakrishna, B. Burfeindt, B. Pettinger, R. Eichberger, and W. Storck, J. Phys. Chem. B **105**, 9245 (2001).
[12] D. Kuciauskas, J. E. Monat, R. Villahermosa, H. B. Gray, N. S. Lewis, and J. K. McCusker, J. Phys. Chem. B **106**, 9347 (2002).
[13] J. Kallioinen, G. Benkö, P. Myllyperkiö, L. Khriahctchev, B. Skårman, R. Wallenberg, M. Tuomikoski, J. E. I. Korppi-Tommola, V. Sundström, and A. P. Yartsev, J. Phys. Chem. B **108**, 6365 (2004).
[14] S. H. Lin, C. H. Chang, K. K. Liang, R. Chang, Y. J. Shiu, J. M. Zhang, T. S. Yang, M. Hayashi, and F. C. Hsu, Adv. Chem. Phys. **121**, 1 (2002).
[15] M. Thoss, I. Kondov, and H. Wang, Chem. Phys. **304**, 169 (2004).
[16] W. Stier and O. Prezhdo, J. Phys. Chem. B **106**, 8047 (2002).
[17] W. Duncan, W. Stier, and O. Prezhdo, J. Am. Chem. Soc. **127**, 794 (2005).
[18] S. Ramakrishna, F. Willig, and V. May, Phys. Rev. B **62**, 16330 (2000).
[19] S. Ramakrishna, F. Willig, and V. May, J. Chem. Phys. **115**, 2743 (2001).
[20] S. Ramakrishna, F. Willig, V. May, and A. Knorr, J. Phys. Chem. B **107**, 607 (2003).
[21] L. Wang and V. May, J. Chem. Phys. **121**, 8039 (2004).
[22] L. Rego and V. Batista, J. Am. Chem. Soc. **125**, 7989 (2003).
[23] B. Fain, S. H. Lin, and N. Hamer, J. Chem. Phys. **91**, 4485 (1989).
[24] L. Wang, R. Ernstorfer, F. Willig, and V. May, J. Phys. Chem. B **109**, 9589 (2005).
[25] B. Burfeindt, T. Hannappel, W. Storck, and F. Willig, J. Phys. Chem. **100**, 16463 (1996).
[26] T. L. Einstein, J. A. Hertz, and J. R. Schrieffer, in *Theory of Chemisorption*, Topics in Current Physics Vol. 19, edited by J. R. Smith (Springer-Verlag, Berlin, 1980), Chap. 7, pp. 183–235.
[27] S. A. Haque, S. Handa, K. Peter, E. Palomares, M. Thelakkat, and J. R. Durrant, Angew. Chem., Int. Ed. **44**, 5740 (2005).
[28] S. H. Lin, J. Chem. Phys. **90**, 7103 (1989).
[29] S. H. Lin, R. G. Alden, C. K. Tang, Y. Fujimura, and F. Sugawara, in *Mode Selective Chemistry*, The Jerusalem Symposia on Quantum Chemistry and Biochemistry Vol. 24, edited by J. Jortner, R. Levine, and B. Pullman (Kluwer, Dordrecht, 1991), pp. 467–484.
[30] Y. Q. Gao, Y. Georgievskii, and R. A. Marcus, J. Chem. Phys. **112**, 3358 (2000).
[31] Y. Q. Gao and R. A. Marcus, J. Chem. Phys. **113**, 6351 (2000).